Microchimica Acta (2021) 188: 214
https://doi.org/10.1007/s00604-021-04875-1

ORIGINAL PAPER

Integrated nicking enzyme-powered numerous-legged DNA walker prepared by rolling circle amplification for fluorescence detection of microRNA

Lihua Wang[1] · Hanqing Zeng[2] · Xiaolan Yang[3] · Chaoming Chen[3] · Shu Ou[3]

Received: 16 January 2021 / Accepted: 20 May 2021 / Published online: 29 May 2021

Abstract

MicroRNAs (miRNAs) have been accepted as promising non-invasive biomarkers for cancer early diagnosis. Developing amplified sensing strategies for detecting ultralow concentration of miRNAs in clinical samples still requires much effort. Herein, an integrated fluorescence biosensor using nicking enzyme-powered numerous-feet DNA walking machine was developed for ultrasensitive detection of miRNA. A long numerous-feet walker produced by target-triggered rolling circle amplification autonomously moves along the defined DNA tracks on gold nanorods (AuNRs) with the help of nicking enzyme, leading to the recovery of fluorescence. This results in an amplified fluorescence signal, typically measured at 518 nm emission wavelength. Benefiting from the long walker that dramatically improves movement range, the homogenous and one-step strategy realizes ultrahigh sensitivity with a limit of detection of 0.8 fM. Furthermore, this walking machine has been successfully used to quantification of miRNA in clinical serum samples. The consistency of the gained results between of the developed strategy and reverse transcription quantitative polymerase chain reaction (RT-qPCR) shows that the sensing method has great promise for tumor diagnostics based on nucleic acid.

Keywords MicroRNA analysis · Numerous-legged walker · Rolling circle amplification · Nicking enzyme-propelled machine · Long movement distance

Introduction

The incidence and mortality of cancer is rapidly increasing. Although tumor biopsies are the most credible technologies in the clinical cancer diagnosis [1], these methods suffer from several disadvantages including the difficulty of attaining samples, invasion that usually yields severe concurrent side effects, sampling bias that cannot react to the heterogeneity and continuous evolution of tumor [2, 3]. Thus, it is important to search new biomarkers with non-invasive and highly sensitive and specific for tumor diagnosis.

MicroRNAs (miRNAs), small single-stranded endogenous non-coding RNA, can regulate physiological function [4, 5]. Studies demonstrated that miRNAs released into fluids (serum, saliva, and cerebrospinal fluid) by tumor cells are potential non-invasive biomarkers for cancer early diagnosis and real time monitoring [6, 7]. For instance, the expression level of miRNA-21 obviously elevated in breast cancer patients and reduced after surgery [8]. Despite miRNAs are novel ideal tumor biomarkers, detecting miRNAs is still a challenge since its low abundance, short length, and high sequence homology [9, 10]. Currently, common methods such as northern blotting, microarray, reverse transcription quantitative polymerase chain reaction (RT-qPCR), and next-generation sequencing have been used for the detection of miRNAs [11–13]. However, these methods undergo either cumbersome experimental operation or low sensitivity [14]. Thus, enormous interest exists in developing new and simple alternative strategies for detecting extremely low concentration of miRNAs in real samples [15, 16].

Lihua Wang and Hanqing Zeng contributed equally to this work.

✉ Shu Ou
oushu321@163.com

[1] Health Management Medical Examination Center, the Second Affiliated Hospital of Chongqing Medical University, Chongqing 404600, China

[2] Department of Hematology, the Second Affiliated Hospital of Chongqing Medical University, Chongqing 404600, China

[3] Department of Neurology, the Fengjie People's Hospital, Fengjie Branch of the Second Affiliated Hospital of Chongqing Medical University, Fengjie County, Chongqing 404600, China

As one of the most appealing building materials, DNA has been applied to assemble many dynamic molecular devices, including DNA walkers, tweezers, and catalytic circuit systems, to sense and enlarge target [17–22]. Among them, DNA walkers have been used to construct various signal amplification strategies for sensing clinical biomarkers [23–25]. In term of typic DNA walkers, the autonomous movement of the walkers along the defined DNA tracks can transfer target information into detectable signals [26–29]. To date, most DNA walkers have only one walking strand, which are called as the single-legged DNA walkers. However, these DNA walkers suffer from several drawbacks such as limited walking distance, slow response kinetics, and premature dissociation from the tracks [30–32]. To achieve high signal gain in a short reaction time, bipedal, tripedal, and four-legged DNA walkers have been developed [33–35]. Although such DNA walkers possess improved walking distance and response rate, the number of "legs" still is relatively limited. Therefore, constructing DNA walkers with more "legs" remains an urgent need.

In this work, we developed an integrated nicking enzyme-powered numerous-legged DNA walker prepared by rolling circle amplification (RCA) on gold nanorods (AuNRs) for ultrasensitive fluorescence detection of miRNA. RCA is one of the commonly used strategies to construct biosensing systems because of its high amplification efficiency [36]. In the presence of miRNA, RCA is triggered, producing a long single-strand containing numbers of repetitive sequences that is regarded as a numerous-feet walker. Then, the long walker stepwise recognizes the FAM-labeled hairpins immobilized on AuNR, resulting in progressively enhanced the binding force of track. After the hairpins are opened, nicking enzymes specifically bind the nicking site to cleave the opened hairpins, simultaneously driving the long walker to further move, therefore generating abundant fluorescence signal for target detection.

Experimental section

Materials and reagents

Oligonucleotides shown in Table S1, H2 labeled with 6-carboxyfluorescein (FAM) and black-hole-quencher 1 (BHQ1), chloroauric acid ($HAuCl_4$), and 10 mM dNTP mixture were purchased from Sangon Biotech (Shanghai, China, https://www.sangon.com). Sodium dodecyl sulfate (SDS), cetyltrimethylammonium bromide (CTAB), and ascorbic acid (AA) were bought from Sigma-Aldrich (https://www.sigmaaldrich.com/). Nicking enzyme (Nb.BbvCI), DNA polymerase (Phi29), T4 DNA ligase, Exonuclease I, and Exonuclease III were supplied by New England Biolabs (https://www.neb.com/). All DNA sequences were annealed before use. All other reagents were of analytical reagent grade. All aqueous solutions were prepared with Milli-Q water (≥18 MΩ, Millipore, http://www.merckmillipore.com/).

Apparatus

The morphology features of AuNRs were characterized by transmission electron microscope (TEM) (Hitachi-7500, Japan, http://www.jeol.co.jp/). UV-vis absorption spectra (Nano-Drop1000, Thermo, USA, http://www.nanodrop.com) were applied to confirm the constructed machine tracks. The fluorescence spectra were obtained from Cary Eclipse Fluorescence Spectrophotometer (Agilent, California, http://www.agilent.com).

Construction of the machine tracks

To build the tracks (hairpins-AuNRs), AuNRs were firstly synthesized following previous reported seed-mediated growth method [37]. The synthesis detail was shown in Supporting Material. The concentration of AuNRs was estimated to be 12.5 nM using UV-Vis spectroscopy [38, 39]. Then, the synthesized AuNRs were functionalized with thiolated DNA hairpins according to previous method [39, 40], and the process was described in Supporting Material.

Preparation of DNA ring for RCA

The mixture including 5′-phosphorylated DNA padlock (100 μM, 1.5 μL) and ligation DNA (100 μM, 3.0 μL) was annealed. After which, T4 DNA ligase (2 μL 50 U), 10 × T4 DNA ligase buffer (2 μL), and 11.5 μL diethylpyrocarbonate (DEPC) water were added into the mixture, and then the mixture was incubated at 16 °C for 24 h followed by heat treating at 65 °C for 15 min to deactivate T4 ligase. Subsequently, 40 U Exo I and 40 U Exo III were added to digest uncirculated DNA. After that, the protein enzymes were further inactivated at 90 °C for 20 min. Finally, the prepared DNA ring was stored at 4 °C for further use.

Fluorescence measurements

To drive the walker system, 2 μL different concentrations of miRNA-21 was added to 18 μL of the mixture consisting of 0.2 U/L Phi29, 0.15 U/L Nb.BbvCI, 200 M dNTP, 2 μL of phi29 reaction buffer, 2 μL of CutSmartTM buffer, 2 μL of hairpins-AuNRs solution, and 2 μL of DNA ring. Then, the mixture was incubation at 37 °C for 1.5 h. Subsequently, the mixture was diluted to 100 μL and then measured. The emission spectrum was recorded from 500 to 600 nm. The maximum fluorescence signal was recorded at 518 nm. The excitation wavelength was set at 480 nm in steps of 1 nm. The emission and excitation slit widths were set at 5 nm. Before

each test, the quartz cell was washed 3 times in 75% ethanol, 3 times in distilled water, and then dried with nitrogen.

miRNA-21 detection in serum samples

The human serum was firstly diluted to 10% in deionized water. Then, different concentrations of miRNA-21 were added into the diluted human serum. The following steps of detection were the same with the detection steps in buffer solution.

Native polyacrylamide gel electrophoresis (PAGE)

Native PAGE was employed for verifying the RCA. The experiment was conducted in 1 × TBE buffer. The PAGE was run for 40 min at 110 V. Then, the gel (8%) was stained with Gel-Red for 30 min and imaged by a Bio-Rad ChemDoc XRS (Bio-Rad, USA, http://www.biorad.com/).

Result and discussion

Operation principle of the biosensor

The detection principle of the biosensor based on nicking enzyme-powered numerous-feet DNA walker is shown in Scheme 1. Hairpins H1 and H2 immobilized on the same AuNR are used to capture the target and act as walking track, respectively. In this method, the target specifically hybridizes and opens H1, leading to the exposure of the lock domain. The exposed domain recognizes the DNA ring to produce a long DNA strand containing many repetitive sequences that is used as a numerous-feet walker with the help of Phi29. Then, the numerous-feet walker binds to the loop domain in H2 successively, forming numbers of double-strands containing cleavage sites for Nb.BbvCI. Hydrolysis of the DNA track can release FAM-tagged fragments from AuNR and leads to the recovery of FAM fluorescence. Subsequently, the numerous-feet walker is released and binds further to the next adjacent track probes to form new cleavage sites. Thus, the autonomous movements of the numerous-feet walker can be driven by nicking enzyme cleavage to release numerous FAM-labeled fragments for detection of miRNA. In the absence of miRNA, the walking machine fails to be activated, and the FAM fluorescence is quenched by AuNR and BHQ1 quenching agent.

Characterization of the machine tracks

To prove the successful construction of the machine tracks, the feature of AuNRs and the binding of the hairpins onto AuNRs were depicted by TEM and UV-vis absorption spectra, respectively. The good dispersity and uniformity of the synthetic AuNRs are clearly seen in Fig. 1A. Analyzing by ImageJ, the average dimension of the synthetic AuNRs is 88.3 nm in length and 15.6 nm in diameter. As shown in Fig. 1B, DNA hairpins solution has a characteristic absorption peak at 260 nm. Compared to DNA hairpins and AuNRs, there is a typical DNA absorption peak in hairpins-AuNRs, demonstrating the successful assembly of hairpins on AuNRs. Furthermore, the zeta potentials of AuNRs and DNA hairpins@AuNRs were conducted, and the results were

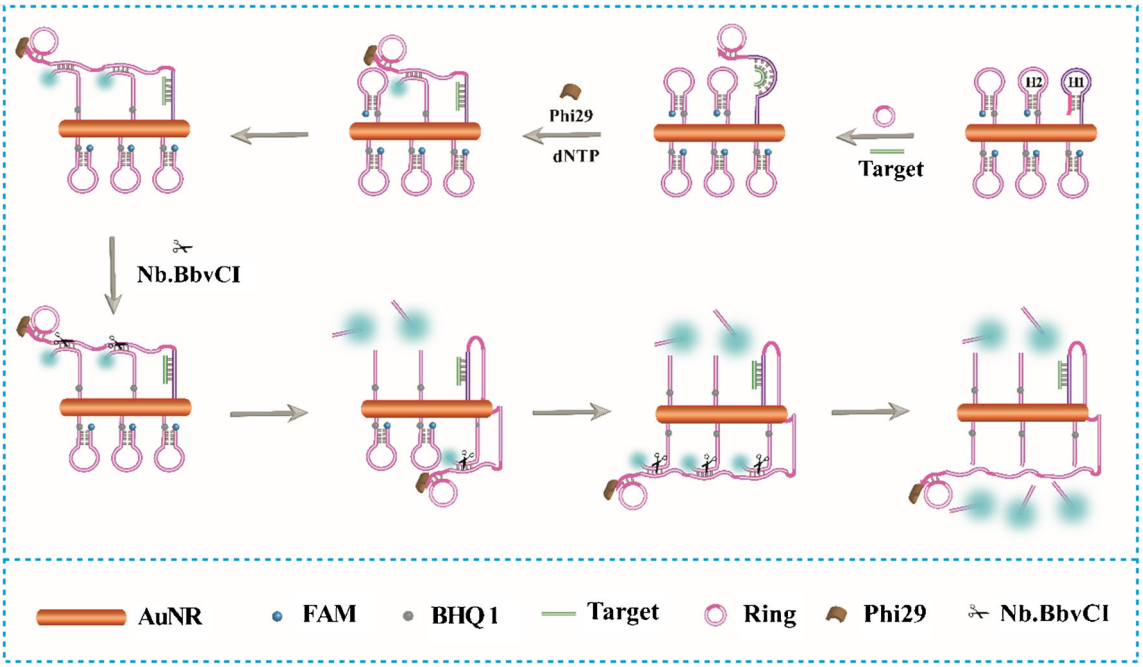

Scheme 1 Schematic illustration of the biosensor using nicking enzyme-powered numerous-legged DNA walker for the detection of miRNA-21

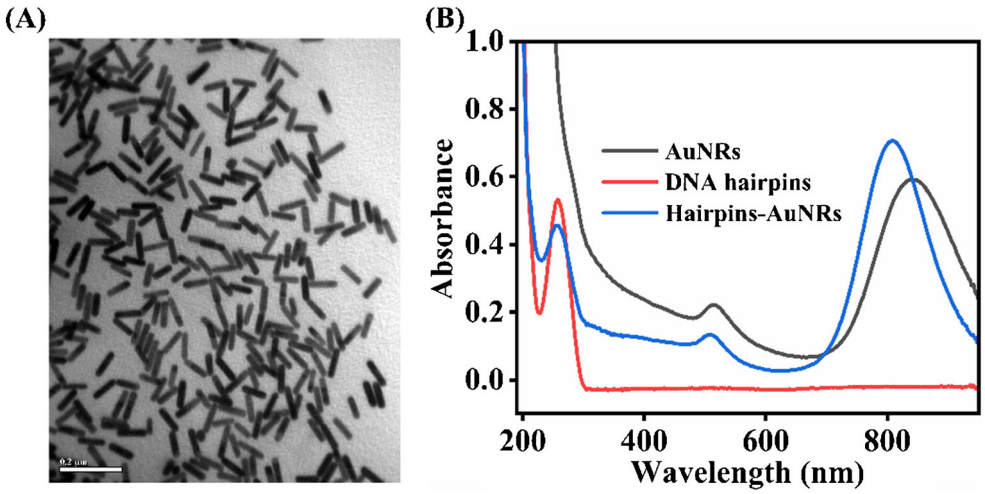

Fig. 1 Characterization of the machine tracks. (A) TEM images of AuNRs. Scale bars: 200 nm. (B) UV-vis spectra of DNA hairpins, AuNRs, and hairpins-AuNRs

shown in Fig. S1. Compared to AuNRs, DNA hairpins@AuNRs exhibits more negative potential, demonstrating the successful binding of DNA hairpins to AuNRs. These results demonstrate that the machine tracks have been constructed as expected. The number of DNA hairpins on AuNR was calculated based on the previously reported methods [31, 41], a liner relationship between fluorescence intensity and concentration of FAM-labeled H1 was gained (Fig. S2). Based on the fluorescence intensity of the supernatant containing superfluous FAM-labeled H1, the amount of DNA hairpins on each AuNR was about 452.

Feasibility of the sensing strategy

The RCA was first verified by native PAGE. As shown in Fig. 2A, the primer stands for the exposed domain of H1, locating in lane 1. Compared with the band of DNA ring (lane 3), a new band with a slower mobility is observed in the mixture of the primer and DNA ring (lane 2), indicating the successful hybridization between the primer and DNA ring. After the incubation of phi29 and dNTPs, many new bands with obviously reduced migration are observed (lane 4), suggesting the generation of long DNA strands by means of RCA.

Furthermore, the fluorescence spectra were recorded in different conditions to confirm the reaction process of the sensing strategy (Fig. 2B). An ignorable signal is observed when the machine tracks (hairpins-AuNRs) is present (curve a), suggesting that the fluorescence of FAM is fully quenched. Upon the DNA ring, Phi29, Nb.BbvCI, and dNTPs are added to the machine tracks solution, the signal has hardly changed (curve b). The result demonstrates that the RCA cannot be activated in the absence of the target, due to the frustrated hybridization of the DNA ring and H1. Thus, the sensing

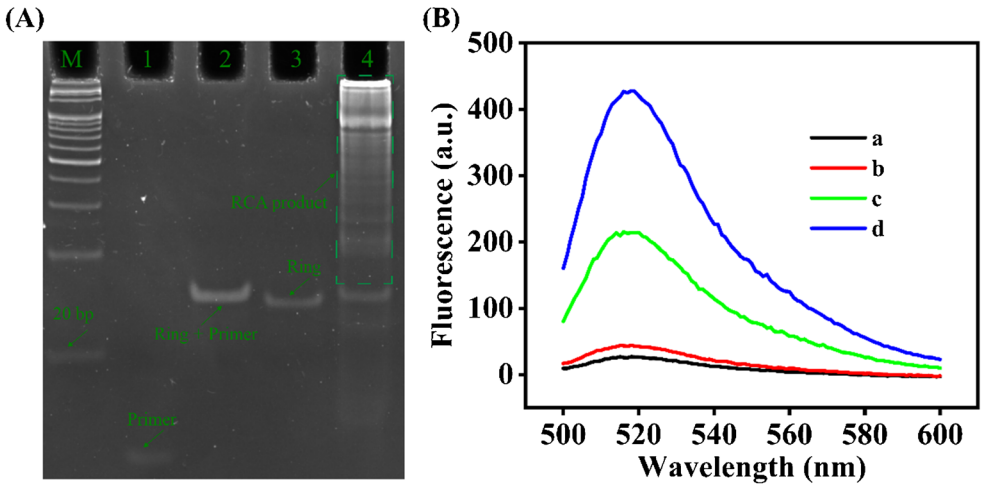

Fig. 2 Feasibility of the sensing strategy. (A) Verification of the reaction process of RCA by PAGE. The concentrations of DNA substrates were 2 μM. The reaction time of RCA was 2.0 h. (B) Fluorescence signal responding to different reaction conditions: (a) the machine tracks, (b) DNA ring + Phi29 + Nb.BbvCI + the machine tracks, (c) target + DNA ring + Phi29 + the machine tracks, and (d) target + DNA ring + Phi29 + Nb.BbvCI + the machine tracks. The concentration of the target was 100 nM. Excitation wavelength: 480 nm and Emission wavelength: 518 nm

strategy has low background noise. Also, an enhanced signal is recorded in the presence of target, DNA ring, Phi29, dNTPs, and the machine tracks (curve c), suggesting that the numerous-feet walker produced by RCA opens the H2, leading to the part recovery of fluorescence. However, when the target exists in the whole sensing system including Nb.BbvCI, Phi29, DNA ring, dNTPs, and the machine tracks, a significant amplified fluorescence signal is seen (curve d). This might be because Nb.BbvCI releases the FAM-labeled sequences from the AuNRs and further propels the movement of the numerous-feet walker, resulting in the decrease of the fluorescence quenching and the increase of the number of the opened H2. The results clearly demonstrate the feasibility of the numerous-feet DNA walking machine for amplified detection of miRNA.

In addition, compared to free H1 and H2, the developed numerous-feet DNA walking machine products significantly enhanced fluorescence signal in the same reaction time (Fig. S3). This is due to that H1 and H2 are integrated on the same AuNR, enhancing the reaction rate of the machine.

Optimization of sensing conditions

To obtain the best sensitivity of the proposed strategy, several reaction conditions were optimized. These conditions included the ratio of H1 to H2, the H1 concentration, the Phi29 concentration, and the reaction time. Since the competitive relation between H1 and H2 during assembly on AuNRs, the concentration ratio of H1 to H2 was first evaluated. As shown in Fig. S4A, with the decrease of the ratio of H1 to H2 from 1/6 to 1/10, the fluorescence intensity gradually enhances and reaches to the peak value at 1/10, suggesting the optimal target recognition efficiency and the number of the DNA track probes. Under the optimal ratio, various H1 concentrations were tested. As illustrated in Fig. S4B, the fluorescence signal undergoes an upward trend from 4.0 to 10.0 μM H1, after which, the signal remains unchanged. Figure S4C shows the change in fluorescence signal with Phi29 concentration from 0.05 to 0.6 U/L. The signal reaches to the maximum value at 0.2 U/L, indicating that the polymerase concentration is adequate to operate RCA. Figure S4D gives information about the fluorescence intensities in different reaction times. The signal improves gradually from 0.5 to 1.5 h, and the maximal signal is gained at 1.5 h. As shown in Fig. S5, the fluorescence signal gradually enhances with the increase of Nb.BbvCI concentration from 0.05 to 0.15 U/L. Then, the signal remains stable. According to these results, the following sensing conditions were used to the subsequent assay: the best ratio of H1 to H2 is 1/10, the incubation time is set at 1.5 h, and the optimal concentrations of H1, Phi29, and Nb.BbvCI are 10.0 μM, 0.2 U/L, and 0.15 U/L, respectively.

Sensitivity of the sensing strategy

Under the optimal sensing conditions, the sensitivity of the strategy was assessed by detecting different target concentrations. As seen in Fig. 3A, there is an ascending trend in fluorescence signal with the augment of miRNA concentrations ranging from 1 fM to 100 nM. When the target concentration is more than 100 nM, the signal has not increased any more. This is due to that 100 nM of target is enough to open all H1 hairpins. The detailed correlation between the variation of fluorescence intensity and the logarithm of target concentration is illustrated in Fig. 3B. A good linear range is from 1 fM to 100 nM with the regression equation as follows: $F = 198.4 + 47.6$ lg C, in which F is the fluorescence intensity, and C stands for the miRNA concentration. The corresponding correlation coefficient is 0.9942. The limit of detection (LOD) of the sensing strategy is calculated to be 0.8 fM based on the average signal of blank plus three times of the standard deviation. In addition, Stern–Volmer equation was used to describe the quenching process of the strategy: $(I_o/If) = 1 + Ksv[quencher]$, where I_o is the fluorescence intensity of the developed method in the absence of quencher, If is the fluorescence intensity of the method in various concentrations of quencher, and Ksv is the Stern–Volmer constant. As shown in

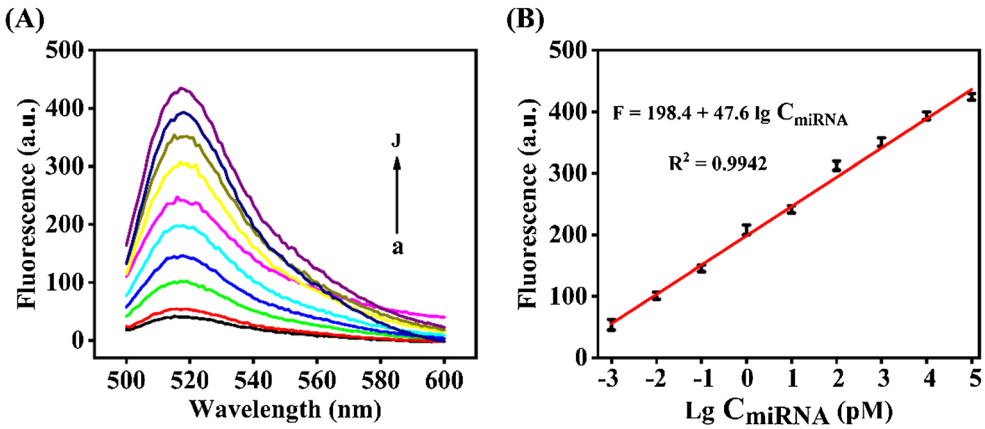

Fig. 3 Evaluation of the sensitivity of the sensing strategy. (A) Fluorescence intensities of the strategy with different miRNA concentrations (a to j: 0 fM, 1 fM, 10 fM, 100 fM, 1 pM, 10 pM, 100 pM, 1 nM, 10 nM, 100 nM). (B) The relationship between fluorescence intensities and the logarithm of miRNA concentrations. All results expressed as mean ± standard variation ($n = 3$). Excitation wavelength: 480 nm and emission wavelength: 518 nm

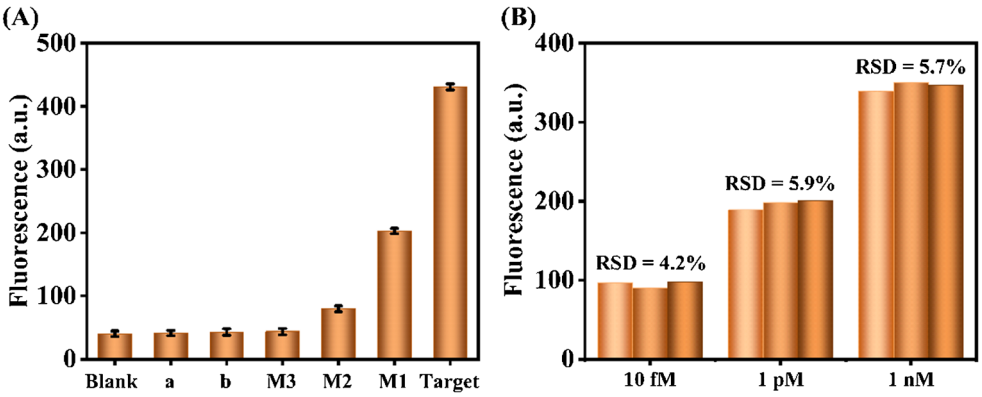

Fig. 4 (A) Evaluation of the specificity of the strategy. The concentrations of all miRNAs are 100 nM. (B) Investigation of the reproducibility of the strategy by detecting different concentration of target miRNA in three individual tests. Excitation wavelength: 480 nm and emission wavelength: 518 nm

Fig. S6, the relationship between I_o/If and quencher concentration is almost linear and Ksv is 0.81, indicating that quenching is static. Compared with the recently reported miRNA fluorescence biosensors based on DNA walkers [42–46], the strategy shows superior sensitivity, wide detection range, and comparable detection time (detail in Table S2). The good analytical performance of the biosensor is attributed to the long movement distance of the developed multiple-legged DNA walker, which has more potential for the detection of trace miRNA in clinical samples.

Specificity and reproducibility investigation

To investigate the specificity of the sensing strategy, the comparative studies between the target miRNA-21 and other analogous miRNAs were performed. These analogous miRNAs included single-base mismatched miRNA-21 (M1), two-base mismatched miRNA-21 (M2), three-base mismatched miRNA-21 (M3), miRNA-122 (a), and miRNA-155 (b). Figure 4A shows the results of the comparative studies. The fluorescence signals of M3, miRNA-122, and miRNA-155 are almost consistent with the blank control. The signal generated by miRNA-21 is about 5.4 times and 2.1 times that of M2 and M1, respectively. These results indicate that the sensing strategy has a good specificity, even can distinguish single-base mismatched. In addition, the reproducibility of the strategy was evaluated by three individual measurements with 10 fM, 1 pM, and 1 nM target miRNA, respectively. The relative standard deviations (RSDs) were 4.2%, 5.9% and 5.7% for the three different concentrations of target miRNA, respectively (Fig. 4B). Considering that the random distribution of the modified hairpins on the AuNRs could influence fluorescence signal, the walker tracks synthesized in three different batches were also used to investigate the reproducibility. The RSD was evaluated as 6.7% responding to 1 pM target. According to these results, the developed sensing strategy has acceptable reproducibility.

Practicability of the fluorescence strategy

To evaluate the practicability of the sensing strategy, standard addition method was conducted in 10% serum samples according to the previously reported papers [32, 34]. The serum samples were diluted to mitigate the strong fluorescence absorption. These serum samples were from different healthy persons. After spiked with different concentrations of miRNA-21, these serum samples were tested by the proposed strategy and RT-qPCR, respectively. As shown in Table S3, the two methods gain the accordant analytical results. The recoveries are between 98.0% and 108.6%, and the RSDs are between 4.9% and 5.7%. These results reveal that the developed sensing strategy has great application value for the early diagnosis of tumor.

Conclusion

In conclusion, a nicking enzyme-propelled numerous-feet DNA walking machine for ultrasensitive detection of miRNA has been developed. Compared with the reported DNA walkers that suffer from untimely derail and limited movement distance, this method is endowed with several obvious advantages. Firstly, the long numerous-feet walker produced by RCA improves the binding force of track, avoiding dissociate prematurely from the track. Secondly, the developed DNA walker has superior mobility by increasing the number of "legs." Thirdly, the target-induced numerous-legged walker and DNA tracks are integrated on the AuNR, which significantly enhances the reaction rate. In the light of this fact that ultrahigh sensitivity and practicability are both realized, the DNA walking machine provides a potential sensing platform to detect biomarkers for cancer diagnosis.

Supplementary Information The online version contains supplementary material available at https://doi.org/10.1007/s00604-021-04875-1.

Funding This work was supported by the Natural Science Foundation Project of Chongqing (cstc2020jcyj-msxmX0611) and the Talent Fund of the Fengjie People's Hospital.

Compliance with ethical standards

Conflict of interest The authors declare that they have no competing interests.

References

1. Hu P, Zhang S, Wu T, Ni D, Fan W, Zhu Y, Qian R, Shi J (2018) Fe-Au nanoparticle-coupling for ultrasensitive detections of circulating tumor DNA. Adv Mater 30(31):e1801690
2. Murtaza M, Dawson SJ, Tsui DW, Gale D, Forshew T, Piskorz AM, Parkinson C, Chin SF, Kingsbury Z, Wong AS, Marass F, Humphray S, Hadfield J, Bentley D, Chin TM, Brenton JD, Caldas C, Rosenfeld N (2013) Non-invasive analysis of acquired resistance to cancer therapy by sequencing of plasma DNA. Nature 497(7447):108–112
3. Jin CE, Koo B, Lee TY, Han K, Lim SB, Park IJ, Shin Y (2018) Simple and low-cost sampling of cell-free nucleic acids from blood plasma for rapid and sensitive detection of circulating tumor DNA. Adv Sci 5(10):1800614
4. van Rooij E, Sutherland LB, Qi X, Richardson JA, Hill J, Olson EN (2007) Control of stress-dependent cardiac growth and gene expression by a microRNA. Science 316(5824):575–579
5. Dong H, Lei J, Ding L, Wen Y, Ju H, Zhang X (2013) MicroRNA: function, detection, and bioanalysis. Chem Rev 113(8):6207–6233
6. Lu J, Getz G, Miska EA, Alvarez-Saavedra E, Lamb J, Peck D, Sweet-Cordero A, Ebert BL, Mak RH, Ferrando AA, Downing JR, Jacks T, Horvitz HR, Golub TR (2005) MicroRNA expression profiles classify human cancers. Nature 435(7043):834–838
7. Rasnic R, Linial N, Linial M (2017) Enhancing identification of cancer types via lowly-expressed microRNAs. Nucleic Acids Res 45(9):5048–5060
8. Du J, Yang S, An D, Hu F, Yuan W, Zhai C, Zhu T (2009) BMP-6 inhibits microRNA-21 expression in breast cancer through repressing deltaEF1 and AP-1. Cell Res 19(4):487–496
9. Li X, Cheng W, Li D, Wu J, Ding X, Cheng Q, Ding S (2016) A novel surface plasmon resonance biosensor for enzyme-free and highly sensitive detection of microRNA based on multi component nucleic acid enzyme (MNAzyme)-mediated catalyzed hairpin assembly. Biosens Bioelectron 80:98–104
10. Kuang Y, Cao J, Xu F, Chen Y (2019) Duplex-specific nuclease-mediated amplification strategy for mass spectrometry quantification of MiRNA-200c in breast cancer stem cells. Anal Chem 91(14):8820–8826
11. Ouyang T, Liu Z, Han Z, Ge Q (2019) MicroRNA detection specificity: recent advances and future perspective. Anal Chem 91(5): 3179–3186
12. Ye J, Xu M, Tian X, Cai S, Zeng S (2019) Research advances in the detection of miRNA. J Pharm Anal 9(4):217–226
13. Zhang C, Miao P, Sun M, Yan M, Liu H (2019) Progress in miRNA detection using graphene material-based biosensors. Small 15(38): e1901867
14. Wang YH, He LL, Huang KJ, Chen YX, Wang SY, Liu ZH, Li D (2019) Recent advances in nanomaterial-based electrochemical and optical sensing platforms for microRNA assays. Analyst 144(9): 2849–2866
15. Masud MK, Umer M, Hossain MSA, Yamauchi Y, Nguyen NT, Shiddiky MJA (2019) Nanoarchitecture frameworks for electrochemical miRNA detection. Trends Biochem Sci 44(5):433–452
16. Deng R, Zhang K, Li J (2017) Isothermal amplification for MicroRNA detection: from the test tube to the cell. Acc Chem Res 50(4):1059–1068
17. Lei S, Liu Z, Xu L, Zou L, Li G, Ye B (2020) A "signal-on" electrochemical biosensor based on DNAzyme-driven bipedal DNA walkers and TdT-mediated cascade signal amplification strategy. Anal Chim Acta 1100:40–46
18. Wang W, Yu S, Huang S, Bi S, Han H, Zhang JR, Lu Y, Zhu JJ (2019) Bioapplications of DNA nanotechnology at the solid-liquid interface. Chem Soc Rev 48(18):4892–4920
19. Li D, Cheng W, Li Y, Xu Y, Li X, Yin Y, Ju H, Ding S (2016) Catalytic hairpin assembly actuated DNA nanotweezer for logic gate building and sensitive enzyme-free biosensing of MicroRNAs. Anal Chem 88(15):7500–7506
20. Huo M, Li S, Zhang P, Feng Y, Liu Y, Wu N, Ju H, Ding L (2019) Nanoamplicon comparator for live-cell microRNA imaging. Anal Chem 91(5):3374–3381
21. Bai M, Chen F, Cao X, Zhao Y, Xue J, Yu X, Fan C, Zhao Y (2020) Intracellular entropy-driven multi-bit DNA computing for tumor progression discrimination. Angew Chem Int Ed 59(32):13267–13272
22. Xue J, Chen F, Bai M, Cao X, Huang P, Zhao Y (2019) All-in-one synchronized DNA nanodevices facilitating multiplexed cell imaging. Anal Chem 91(7):4696–4701
23. Xiao M, Zou K, Li L, Wang L, Tian Y, Fan C, Pei H (2019) Stochastic DNA walkers in droplets for super-multiplexed bacterial phenotype detection. Angew Chem Int Ed 58(43):15448–15454
24. Xu M, Zhuang J, Jiang X, Liu X, Tang D (2019) A three-dimensional DNA walker amplified FRET sensor for detection of telomerase activity based on the MnO_2 nanosheet-upconversion nanoparticle sensing platform. Chem Commun 55(66):9857–9860
25. Zheng J, Ji X, Du M, Tian S, He Z (2018) Rational construction of a DNA nanomachine for HIV nucleic acids ultrasensitive sensing. Nanoscale 10(36):17206–17211
26. Jung C, Allen PB, Ellington AD (2017) A simple, cleated DNA walker that hangs on to surfaces. ACS Nano 11(8):8047–8054
27. Škugor M, Valero J, Murayama K, Centola M, Asanuma H, Famulok M (2019) Orthogonally photocontrolled non-autonomous DNA walker. Angew Chem Int Ed 58(21):6948–6951
28. Qu X, Zhu D, Yao G, Su S, Chao J, Liu H, Zuo X, Wang L, Shi J, Wang L, Huang W, Pei H, Fan C (2017) An exonuclease III-powered, on-particle stochastic DNA walker. Angew Chem Int Ed 56(7):1855–1858
29. Peng H, Li XF, Zhang H, Le XC (2017) A microRNA-initiated DNAzyme motor operating in living cells. Nat Commun 8:14378
30. Xu Z, Chang Y, Chai Y, Wang H, Yuan R (2019) Ultrasensitive electrochemiluminescence biosensor for speedy detection of microRNA based on a DNA rolling machine and target recycling. Anal Chem 91(7):4883–4888
31. Li D, Xu Y, Fan L, Shen B, Ding X, Yuan R, Li X, Chen W (2020) Target-driven rolling walker based electrochemical biosensor for ultrasensitive detection of circulating tumor DNA using doxorubicin@tetrahedron-Au tags. Biosens Bioelectron 148: 111826
32. Wu N, Wang K, Wang YT, Chen ML, Chen XW, Yang T, Wang JH (2020) Three-dimensional DNA nanomachine biosensor by integrating DNA walker and rolling machine cascade amplification for ultrasensitive detection of cancer-related gene. Anal Chem 92(16):11111–11118
33. Liu C, Hu Y, Pan Q, Yi J, Zhang J, He M, He M, Nie C, Chen T, Chu X (2020) Photocontrolled and self-powered bipedal DNA walking machine for intracellular microRNA imaging. Chem Commun 56(24):3496–3499
34. Wang L, Liu P, Liu Z, Zhao K, Ye S, Liang G, Zhu JJ (2020) Simple tripedal DNA walker prepared by target-triggered catalytic hairpin assembly for ultrasensitive electrochemiluminescence detection of microRNA. ACS Sens 5(11):3584–3590

35. Yao D, Bhadra S, Xiong E, Liang H, Ellington AD, Jung C (2020) Dynamic programming of a DNA walker controlled by protons. ACS Nano 14(4):4007–4013
36. Wang L, Deng R, Li J (2015) Target-fueled DNA walker for highly selective miRNA detection. Chem Sci 6(12):6777–6782
37. Lan X, Chen Z, Dai G, Lu X, Ni W, Wang Q (2013) Bifacial DNA origami-directed discrete, three-dimensional, anisotropic plasmonic nanoarchitectures with tailored optical chirality. J Am Chem Soc 135(31):11441–11444
38. Orendorff CJ, Murphy CJ (2006) Quantitation of metal content in the silver-assisted growth of gold nanorods. J Phys Chem B 110(9): 3990–3994
39. Liu B, Song C, Zhu D, Wang X, Zhao M, Yang Y, Zhang Y, Su S, Shi J, Chao J, Liu H, Zhao Y, Fan C, Wang L (2017) DNA-origami-based assembly of anisotropic plasmonic gold nanostructures. Small 13(23):1603991
40. Shen C, Lan X, Lu X, Meyer TA, Ni W, Ke Y, Wang Q (2016) Site-specific surface functionalization of gold nanorods using DNA origami clamps. J Am Chem Soc 138(6):1764–1767
41. Huang J, Zhu L, Ju H, Lei J (2019) Telomerase triggered DNA Walker with a superhairpin structure for human telomerase activity sensing. Anal Chem 91(11):6981–6985
42. Yang T, Fang J, Guo Y, Sheng S, Pu Q, Zhang L, Ou X, Dai L, Xie G (2019) Fluorometric determination of microRNA by using an entropy-driven three-dimensional DNA walking machine based on a catalytic hairpin assembly reaction on polystyrene microspheres. Mikrochim Acta 186(8):574
43. Li Q, Liang X, Mu X, Tan L, Lu J, Hu K, Zhao S, Tian J (2020) Ratiometric fluorescent 3D DNA walker and catalyzed hairpin assembly for determination of microRNA. Mikrochim Acta 187(6): 365
44. Li D, Luo Z, An H, Yang E, Wu M, Huang Z, Duan Y (2020) Polyadenine regulated DNA density on AuNPs to construct efficient DNA walker for microRNA-21 detection. Talanta 217:121056
45. Yang L, Fang J, Li J, Ou X, Zhang L, Wang Y, Weng Z, Xie G (2021) An integrated fluorescence biosensor for microRNA detection based on exponential amplification reaction-triggered three-dimensional bipedal DNA walkers. Anal Chim Acta 1143:157–165
46. Hu M, Mao D, Liu X, Ren L, Zhou M, Chen X, Zhu X (2019) An all-in-one homogeneous DNA walking nanomachine and its application for intracellular analysis of miRNA. Theranostics 9(20): 5914–5923